Available online at www.sciencedirect.com
ScienceDirect
Journal of Hazardous Materials 147 (2007) 971–978
Journal of Hazardous Materials
www.elsevier.com/locate/jhazmat

# Transition state kinetics of Hg(II) adsorption at gibbsite–water interface

Rohan Weerasooriya [a,b,*], Heinz J. Tobschall [a], Wasana Seneviratne [a], Atula Bandara [c]

[a] *Institut für Geologie und Mineralogie, Lehrstuhl für Angewandte Geologie, Friedrich-Alexander Universität Erlangen-Nuremberg, Schlossgarten 5, D 91054 Erlangen, Germany*
[b] *CML, Institute of Fundamental Studies, Kandy, Sri Lanka*
[c] *Department of Chemistry, University of Peradeniya, Peradeniya, Sri Lanka*

Received 16 May 2006; received in revised form 10 November 2006; accepted 26 January 2007
Available online 6 February 2007

**Abstract**

Kinetics of adsorption plays a pivotal factor in determining the bio-availability and mobility of Hg(II) in the environment. The kinetics of Hg(II) adsorption on gibbsite was examined as a function of pH, temperature and electrolyte type. Adsorption of Hg(II) was highly non-linear where the rate of Hg(II) retention was rapid initially and was followed by gradual or somewhat slow retention behavior with increasing contact time. The respective rate constants designated as $k_1$ (S-1: fast step) and $k_2$ (S-2: slow step). Always $k_1$ follows the order: $k_1^{ClO_4} \geq k_1^{(NO_3)_4} \gg k_1^{Cl}$. Such a relationship was not observed for the S-2 route. A two-step reaction model with pseudo-first order kinetics successfully described the adsorption rates of Hg(II) on gibbsite. Arrhenius and Erying models determined the thermodynamic parameters at activation states, which correspond to S-1 and S-2 routes. In a given system, always the activation energies showed a decrease with the pH. Gibbs free energy ($\Delta G^{\#}$), enthalpy ($\Delta H^{\#}$), and entropy ($\Delta S^{\#}$) values of activation states were almost similar both in $NaClO_4$ and $NaNO_3$ which signal a similar Hg(II) adsorptive mechanism on gibbsite. The configurations of different Hg(II)-surface complexes were elucidated by transmission vibration spectroscopy.


*Keywords:* Mercury(II); Arrhenius model; Erying Model; Adsorption kinetics

## 1. Introduction

Mercury is a toxic, carcinogenic, mutagenic and teratogenic element that has a complex chemistry in the environment [1–5]. Mercury exists in three oxidation states, which are 0 (i.e. $Hg^0$), I (i.e. $Hg_2^+$), and II (i.e. $Hg^{2+}$, hereafter Hg(II)). Out of these oxidation states, the $Hg^0$ is volatile and is prevalent in atmosphere [5]. The Hg(II) is the most stable in nature; it is a soft Lewis acid. According to Pearson's hard and soft acid–base theory, it complexes strongly with S-containing ligands [6]. The key factor determining the concentration of Hg(II) in biota is the methylmercury concentration in water, which is controlled by net methylation and demethylation processes [7]. Complexation and sorption of the precursor Hg(II) by ligands and solid substrates may inhibit the production of methylmercury [7,8]. Because of its acute toxicity, the US Environmental Protection Agency (EPA) published ambient water quality criteria recommendations for methylmercury for the protection of people who eat fish and shellfish. This criterion, 0.3 mg methylmercury/kg fish tissue wet weight, marks EPA's first issuance of a water quality criterion expressed as a fish and shellfish tissue value rather than as an ambient water column value [9].

A wide array of heterogeneous complexants such as humic substances (HS), mineral surfaces and bacterial ex-polymers is ubiquitous in aquatic environment. When compared with the high metal binding capacity of HS, the transport, toxicity and fate of Hg(II) (and other metal ions as well) in aquifers are controlled in part by sorption/desorption on hydrous metal oxides and clays [10,11]. However, elucidation of mechanistic behavior of Hg(II) adsorption on soils, sediments or aquifers is arduous due to their inherent complexity. Therefore, much attention was paid to quantify Hg(II) on well-characterized mineral phases that dominate in nature. The rationale here is to consider these discrete phases as 'building blocks' of natural solid substrates in that they could be combined in such a way to identify dominate sorptive surfaces [12]. Along these lines, there are substantial data available on Hg(II) sorption for iron hydrous oxides [13

* Corresponding author at: CML, Institute of Fundamental Studies, Kandy, Sri Lanka. Tel.: +94 81 2232002x24; fax: +94 81 2232131.
*E-mail address:* rweerasooriya@hotmail.com (R. Weerasooriya).

0304-3894/$ – see front matter © 2007 Elsevier B.V. All rights reserved.
doi:10.1016/j.jhazmat.2007.01.134

and references therein]. Similar data on gibbsite or other metal (i.e. Mn and Si) hydrous oxides is comparably low [14–17]. Further, available data do not pay sufficient attention to the examination of kinetic aspects of Hg(II) adsorption on gibbsite or similar solids. Sarkar et al. [14] had shown that kinetic of Hg(II) adsorption on gibbsite is characterized by a rapid step (within 1 h) followed by a slow step when equilibrated for 48 h. Recently, Kim et al. [15,16] noted by in situ spectroscopy that Hg(II) showed a strong affinity for bayerite, an structural analog of gibbsite, which forms inner-sphere complexes. Very recently, we have shown that Hg(II) adsorption kinetics on gibbsite can be characterized by three distinct zones in NaCl, $NaNO_3$, or $NaClO_4$. These zones are designated as a rapid Hg(II) uptake and reversible zone, a slow Hg(II) plateau and reversible zone followed by a rapid Hg(II) uptake and irreversible zone [17]. However, no detail assessment of Hg(II) adsorption kinetics on gibbsite were done in any of these investigations.

A systematic investigation into the kinetics of the Hg(II) adsorption is crucial for a thorough understanding of its mobility in the environment [10]. In this research, kinetics of Hg(II) adsorption on gibbsite as a function of pH, temperature and electrolyte type was examined by a simple multi-step kinetic model. The transition state thermodynamics of the Hg(II)–gibbsite complexes, i.e. enthalpy ($\Delta H^{\#}$), entropy ($\Delta S^{\#}$), and Gibbs energy ($\Delta G^{\#}$) were calculated in $NaNO_3$, $NaClO_4$, and NaCl according to Arrhenius and Erying models.

## 2. Materials and methods

### 2.1. Materials

Unless otherwise mentioned all chemicals were from Sigma–Aldrich (USA) or Merck (Germany). Water was purified with a mixed bed resin to remove any anionic or cationic contaminant traces before distillation. Thousand mg $L^{-1}$ stock solutions of Hg(II) were prepared either with high purity $Hg(ClO_4)_2{\cdot}4H_2O$ or $Hg(NO_3)_2{\cdot}H_2O$. ALCOA (Australia) gibbsite samples were used as received. De-ionized, distilled water was used for all sample preparations. The physico-chemical parameters of gibbsite used were given below [18,19]:

| Parameter | Value |
|---|---|
| Surface area, $A_{sp}$ ($m^2$/g) | 13 |
| Particle size (μm) | 6 |
| Site density[a], $N_s$ (sites/$nm^2$) | 8.11 |
| $pH_{zpc}$ | 8.7 ($NaClO_4$)<br>8.9 ($NaNO_3$)<br>8.7 (NaCl) |

[a] Site concentration = $[(A_{sp}N_s a)/Na] \times 10^{18}$ sites/mol, where $a$ is the solid content in g $L^{-1}$.

All pH adjustments were made with pre-calibrated acids or 0.4820 M NaOH. Pre-calibrated acids used were 0.822 M $HClO_4$, 0.7951 M $HNO_3$ or 0.8722 M HCl. The selection of different acids was done to obtain a similar anion as with background electrolyte used in the experiments.

### 2.2. Methods

Chemical kinetics of Hg(II) adsorption on gibbsite was determined as a function of pH, temperature and background electrolyte type using a series of batch experiments. Preparation of gibbsite–water slurry, typically 2 g $L^{-1}$, for a chemical kinetics study was carried out according to following method. A weighted quantity of gibbsite was homogenized adding a small amount of water with a ceramic mortar and pestle. The paste was transferred to a water-jacketed cell, which contains the electrolyte chosen. The electrolytes used were $NaNO_3$, $NaClO_4$ or NaCl. The reaction vessel was tightly capped with a lid, which had provision for gas outlets, sampling, pH and temperature probes. The reaction cell was always maintained at desired temperature using a water-driven temperature regulator (Advantec, Thermo Cool LCH-130F, Japan). The solid suspension was stirred continuously. All pH adjustments were made between 3 and 8 with pre-calibrated acids (0.822 M $HClO_4$, 0.7951 M $HNO_3$ or 0.8722 M HCl) or a base (0.4820 M NaOH). The suspension was spiked with 1000 μM Hg(II) to yield final concentration of Hg(II) as 2 μM. In most cases, the pH adjustments and Hg(II) spiking were done with solutions containing anionic constituents similar to the background electrolyte used in the hydroxalation. In 0.01 M NaCl systems, however a 1000 μM $HgNO_3$ stock solution was used for spiking. This step was taken due to low solubility of Hg(II) salts. At pre-defined time intervals, samples (5 mL aliquots) were syringed out, and filtered into acidified tubes using 0.45 μm disposable filters for immediate solid–solution separation. All samples were prepared in triplicates. Adsorbed Hg(II) was calculated from the difference between Hg(II) initially added to the system and that remaining in the solution after a pre-defined time interval. The dilution induced by the pH controls were considered while computing the amount of Hg(II) adsorbed.

Bonding of Hg(II) on gibbsite was examined by Fourier transformed infra-red spectroscopy (FT-IR). The Hg(II) adsorption on gibbsite for FT-IR spectroscopic analyses were performed by mixing a 2 g $L^{-1}$ gibbsite suspension in desired electrolyte with 2 μM Hg(II). The solid samples were separated by centrifugation at 10,000 rpm for 15 min, which was followed by washing the solid substrate several times with distilled water. The pH of the water was adjusted to the value of the system being examined. The samples were dried at 298 K and these samples were stored in desiccators prior pellets were prepared for IR analysis. KBr pellets of 1 cm diameter and constant weight were prepared by mixing KBr and the solid samples in a 10:1 ratio and the spectra were measured in 400–4000 $cm^{-1}$ region. In spectral de-convolution, the parameters, i.e. frequency, peak width and amplitude, were adjusted to achieve the best fit, and in all cases, 99.9% of the spectrum was reproduced.

### 2.3. Analytical methods

The pH of the well-stirred suspension was measured with an auto-titrator (Metrohm 702M Titrino, Switzerland) with a Ross sure-flow combined pH electrode (Orion 81-63, USA). The electrode was calibrated using three buffers at pH 4.000, 7.001, and

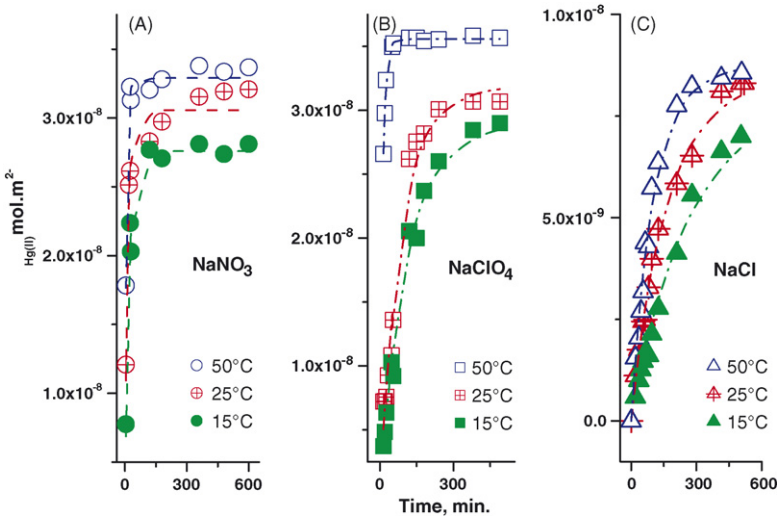


Fig. 1. Variation of Hg(II) adsorption density as a function of equilibration time, temperature and background electrolyte type at pH 5.5. (A) Hg(II)–gibbsite in 0.01 M $NaNO_3$; (B) Hg(II)–gibbsite in 0.01 M $NaClO_4$; (C) Hg(II)–gibbsite in 0.01 M NaCl. Gibbsite, 2 g $L^{-1}$; initial [Hg(II)], 2 μM. Dotted and dashed lines show calculations done according to two-step pseudo-first order model. Similar data were obtained at pH 3.1, 4.2 and 7.1 (details were given in Supporting Information). The portion of the data set corresponding to temperature 298 K were from Ref. [17].

10.01. The Hg(II) analyses were carried out by the cold-vapor technique using a 3 g $L^{-1}$ $NaBH_4$ + 3 g $L^{-1}$ NaOH and 3 M HCl as reducing agent, and an atomic absorption spectrophotometer (GBC 933A, Australia), fitted with the continuous flow hydride generator(GBC HG 3000, Australia). The $Hg^0$ vapor was sparged from solution with $N_2$ into the vapor cell and was determined at 253.7 nm. Always spiked recoveries of Hg for water samples varied from 95 to 105%. IR spectra at transmission mode were collected at 4 $cm^{-1}$ resolution with a FT-IR spectrophotometer with built-in data processing facility (JASCO 410, Japan).

## 3. Results and discussion

### 3.1. Hg(II) adsorption kinetics

Previously, we examined the Hg(II) sorption and desorption on gibbsite in the presence of different electrolytes, i.e. $NaNO_3$, $NaClO_4$ or NaCl at pH 5.5 and 298 K. In all cases the Hg(II) sorption first increased and then reached a plateau which was followed by an enhanced sorption with further increase of contact time, $t_C$. When $t_C < 3$ h, almost 98% of fixed Hg(II) by the solid was recovered, and the sorption mechanism was assumed to be governed by adsorption [17]. Under these circumstances, the Hg(II) adsorption was modeled according to Langmuir (in 0.01 M $NaNO_3$ or 0.01 M $NaClO_4$) or Hill (in 0.01 M NaCl) equation assuming homogeneous sites [17].

As shown in Fig. 1(A–C) the $\Gamma_{Hg(II)}$ on gibbsite as a function of contact time ($t_C$) and temperature was determined in 0.01 M $NaNO_3$, 0.01 M $NaClO_4$ and 0.01 M NaCl at pH 5.5. Similar experiments were carried out at pH 3.1, 4.2 and 7.1 and the details are found under the Supplementary Materials (Fig. 1S). Our data showed that initially $\Gamma_{Hg(II)}$ increased rapidly and more slowly afterwards. In most cases, an apparent plateau was reached within first 20–30 min. The $\Gamma_{Hg(II)}$ values at the onset of plateau were noted ad designated as optimal adsorption density, i.e. $\Gamma^{i,0}_{Hg(II)}$ (Table 1). According to the data shown in Table 1, at a given pH and temperature, $\Gamma^{i,0}_{Hg(II)}$ values in $NaNO_3$ and $NaClO_4$ are comparable; in the presence of $Cl^-$, the $\Gamma^{i,0}_{Hg(II)}$ values reduced almost by about 10-fold. Therefore, $\Gamma^{i,0}_{Hg(II)}$ varied with the electrolyte type according to following order: $\Gamma^{ClO_4,0}_{Hg(II)} \cong \Gamma^{NO_3,0}_{Hg(II)} \gg \Gamma^{Cl,0}_{Hg(II)}$. As shown elsewhere [14,15], out

Table 1
Calculated $\Gamma^{i,0}_{Hg(II)}$ (maximum Hg(II) adsorption density) values as a function of pH, temperature and electrolyte type

| pH | Optimal adsorption density, $\Gamma^0_{max}$ (mol $m^{-2}$) | | | | | | | | |
|---|---|---|---|---|---|---|---|---|---|
| | $NaNO_3$ | | | $NaClO_4$ | | | NaCl | | |
| | 288 K | 298 K | 323 K | 288 K | 298 K | 323 K | 288 K | 298 K | 323 K |
| 3.1 | 1.70E−08 | 1.80E−08 | 1.95E−08 | 1.20E−08 | 1.81E−08 | 2.10E−08 | 1.70E−09 | 1.89E−09 | 2.34E−09 |
| 4.2 | 1.77E−08 | 2.00E−08 | 2.20E−08 | 2.72E−08 | 2.94E−08 | 3.00E−08 | 1.87E−09 | 2.01E−09 | 2.45E−09 |
| 5.5 | 2.76E−08 | 3.06E−08 | 3.29E−08 | 2.88E−08 | 3.18E−08 | 3.56E−08 | 7.80E−09 | 8.35E−09 | 3.56E−09 |
| 7.1 | 2.73E−08 | 3.07E−08 | 3.29E−08 | 2.90E−08 | 3.22E−08 | 3.62E−08 | 1.87E−09 | 2.01E−09 | 8.70E−09 |

The calculations were done according to two-step kinetic model. The $\Gamma^{i,0}_{Hg(II)}$ correspond to $A^i_1 + A^i_2 = \Gamma^{i,e}_{Hg(II)}$; $A^i_1$ and $A^i_2$ are constants. At $t = 0$, $A^i_1 + A^i_2 = \Gamma^{i,0}_{Hg(II)}$ so that $\Gamma^{t,i}_{Hg(II)} = 0$ (see text for details).

of seven chemical species examined (species: $Hg^{2+}$, $HgOH^+$, $Hg(OH)_2$, $Hg(OH)_3^-$, $Hg(OH)_4^{2-}$, $Hg(NO_3)_2^0$, $HgNO_3^-$) the $Hg(OH)_2^0$ is dominant in the pH range of natural waters, i.e. pH 4 to 10. At low pH (<2) $Hg(H_2O)_6^{2+}$ is dominant. When the pH is raised, the $Hg(OH)^+$ becomes dominant representing about 17% at pH 3.1. When the pH is raised further, the conversion of $Hg(OH)^+ \rightarrow Hg(OH)_2^0$ was readily occurred. In the presence of $Cl^-$ the distribution pattern of Hg(II) species changed significantly due to its complexing ability with Hg(II) [16]. When $[Cl^-] = 10^{-2}$ M, out of nine species examined (species: $HgOH^+$, $Hg(OH)_2^0$, $Hg(OH)_3^-$, $Hg(OH)_4^-$, $HgCl^+$, $HgCl_2^0$, $HgCl_3^-$, $HgCl_4^{2-}$, and $HgClOH^0$), the $HgCl_2^0$ has become the dominant species throughout the pH between 4 and 8. The activity of $HgOHCl^0$ species becomes evident from pH 5.7 and upward. The $HgCl_2^0$ seems to play an inert role in surface bonding [16]; however, $HgOHCl^0$ shows some affinity for gibbsite. This is largely due to charge asymmetry of the $HgOHCl^0$ that resulted by the presence of $Cl^-$ and $OH^-$ radicals. Possibility of the precipitation of Hg(II) as $Hg(OH)_{2,solid}$ or $HgCl_{2,solid}$ in different electrolytes, particularly at alkaline pH (>7) was examined by a simple calculation by ECOSAT code [20]. As shown in the table, negative SI values indicate that the system is always unsaturated with respect to $HgCl_{2,solid}$, or $Hg(OH)_{2,solid}$ precipitation when initial [Hg(II)] = 2 μM.

| $I$ (M) | Saturation index (SI)[a] | |
|---|---|---|
| | $HgCl_{2,solid}$ | $Hg(OH)_{2,solid}$ |
| 0.1 | −3.45 to −10.0 | −1.34 to −2.09 |
| 0.01 | −3.18 to −11.0 | −1.34 to −2.09 |
| 0.001 | −3.15 to −13.8 | −9.41 to −2.09 |

[a] SI range corresponds to pH between 3 and 9. Thermodynamic data were used from the ECOSAT built-in database.

It was proposed that ion adsorption on soils can be explained by three concurrent reactions, namely, a rapid and reversible reaction, a slow and reversible reaction, and an irreversible reaction [21]. A similar behavior was noted for Hg(II) adsorption kinetics on gibbsite at extended contact time, $t_C$ [17]. Presently, $t_C$ was restricted to 3 h. This stringent condition assured that Hg(II)–gibbsite interactions are largely characterized by both rapid and slow reversible reaction series [22,23]. Further, the rapid adsorption to the external surface of gibbsite (hereafter S-1 step) is followed by slow sorption of the Hg(II) along surface sites on the micro pore walls (hereafter S-2 step) which eventually reaches an apparent plateau (Fig. 1(A–C)). These arguments do not necessarily imply that S-1 and S-2 steps occur consecutively. The data shown are not sufficient to demarcate different Hg(II) adsorption steps, i.e. S-1 versus and S-2; since S-1 is always included in the overall process; hence, only rate comparisons among different systems is possible [24].

### 3.2. Modeling Hg(II) adsorption kinetics

In all experiments, the $\left(\sum_{total}[> AlOH]/[Hg(II)]\right)$ ratio was kept around ~100, which implies when compared to [Hg(II)], the activity of $\sum_{total}(> AlOH)$ is essentially a constant. Therefore, the kinetics of Hg(II) adsorption on gibbsite can be modeled assuming two-step pseudo-first order kinetics [25]:

$$\Gamma^{t,i}_{Hg(II)} = \Gamma^{i,0}_{Hg(II)} - A^i_1 e^{-k^i_{1t}} - A^i_2 e^{-k^i_{2t}} \quad (1)$$

Here $\Gamma^{t,i}_{Hg(II)}$ and $\Gamma^{i,0}_{Hg(II)}$ are the adsorption densities at a given time $t$, and at optimal conditions, respectively. The data shown in Table 1 were used as $\Gamma^{i,0}_{Hg(II)}$ values. The $k^i_1$ and $k^i_2$ are the rate constants of S-1 and S-2, respectively; $A^i_1$ and $A^i_2$ are their pre-exponential amplitude terms. At $t = 0$, $A^i_1 + A^i_2 = \Gamma^{i,0}_{Hg(II)}$ so that $\Gamma^{t,i}_{Hg(II)} = 0$. The superscript, $i$ denotes electrolyte, i.e. $NaNO_3$, $NaClO_4$ or NaCl, used. As time proceeds, the $\Gamma^{t,i}_{Hg(II)}$ values showed a rapid decline, which reached zero asymptotically. The experimental data were treated numerically by a non-linear optimization algorithm for estimating $k^i_1$, $k^i_2$, $A^i_1$ and $A^i_2$. The modeled Hg(II) adsorption data calculated in three background electrolytes are shown in Fig. 1(A–C) as dotted lines. In all cases, the experimental data fitted well with this kinetic model ($P < 0.01$). Always, $A^i_1 \gg A^i_2$ and $k^i_1 \gg k^i_2$ which show dominance of S-1 over S-2 on Hg(II) adsorption. The initial binding of Hg(II) on gibbsite is thought to occur by removing surface-bonded water molecules on gibbsite as discussed in Section 3.4. This step is considered fast (i.e. S-1). The re-organization of the bounded Hg(II)-surface species is thought comparably slow (i.e. S-2).

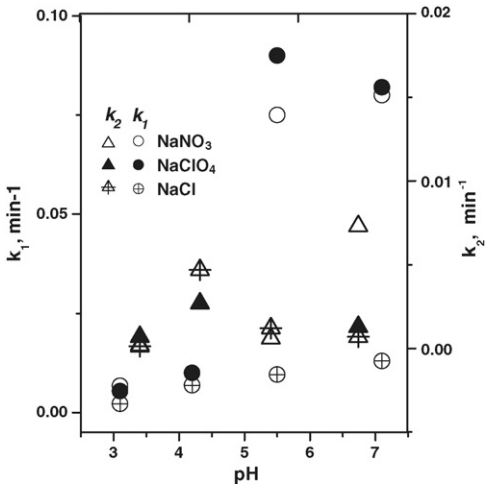


Fig. 2. Variation of rate constants of Hg(II) adsorption of gibbsite as a function of pH at 298 K. Similar plots were obtained (not shown) at 288 and 323 K. Gibbsite, 2 g $L^{-1}$; initial [Hg(II)], 2 μM.

Fig. 2 shows the variation of $k^i_1$ and $k^i_2$ as a function of pH. Both rate constants showed a strong pH dependency. The $k^i_1$ showed a monotonous increase with the pH. At a given pH and temperature, the $k_1$ values follow the order: $k^{ClO_4}_1 \geq k^{(NO_3)_4}_1 \gg k^{Cl}_1$. The ratios of $\left(k^{pH=7.1}_1/k^{pH=3.1}_1\right)_{ClO_4}$, $\left(k^{pH=7.1}_1/k^{pH=3.1}_1\right)_{NO_3}$, and $\left(k^{pH=7.1}_1/k^{pH=3.1}_1\right)_{Cl}$ at pH 3.1 and 7.1 were 12, 15 and 69, respectively. A similar conclusion cannot however be made with respect to S-2.

According to surface complex theory when background electrolytes are non-bonding, gibbsite exhibits three types of surface species, namely >AlOH, $>AlO^-$ and $>AlOH_2^+$. In $NaNO_3$,

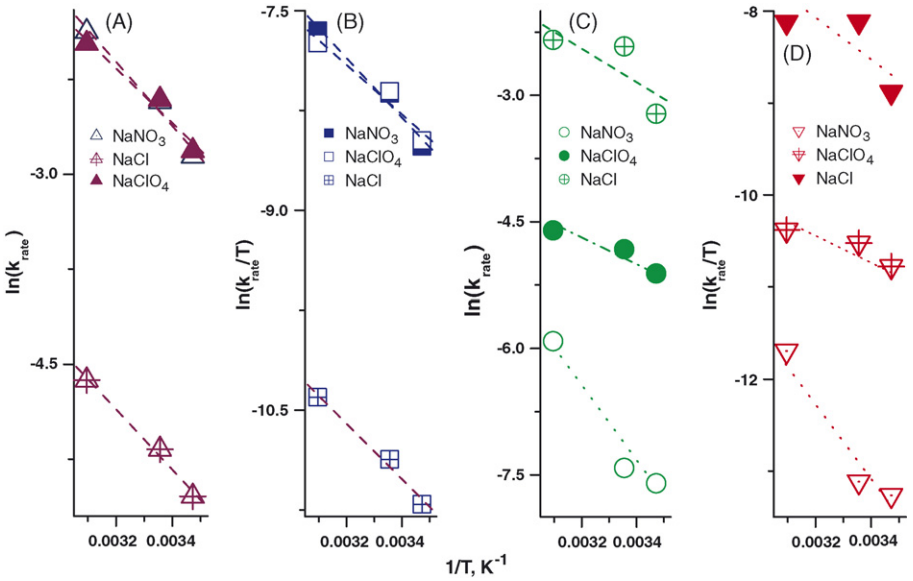


Fig. 3. Arrhenius and Erying plots of Hg(II) adsorption on gibbsite as a function of temperature and electrolyte type at pH 5.5. (A) Arrhenius plot of rapid step of Hg(II) adsorption (S-1); (B) Arrhenius plots of slow step of Hg(II) adsorption (S-2); (C) Erying plot of S-1; (D) Erying plot of S-2. Rate constants of S-1 and S-2 were determined from the data shown in Fig. 1. The data points of $NaClO_4$ and $NaNO_3$ coincided, during S-1. However, such a conclusion cannot readily be made for S-2. Solid content, 2 g $L^{-1}$; initial [Hg(II)], 2 μM. The dotted and dashed lines indicate linear fits conducted to calculate thermodynamic parameters at transition state. As shown in Supporting Information, Fig. 3S similar plots were obtained at pH 3.1, 4.2 and 7.1.

$NaClO_4$, or NaCl, the $pH_{zpc}$ of gibbsite is always >8 [19,24]; thus the surface sites are positively charged between pH 3 and 7. According to diffused-layer model calculations, the ($[>AlOH_2^+]/[>AlO^-]$) ratio was decreased significantly when pH varied from 4 to 7.1. This indicates that the relative concentration of $[>AlOH_2^+]$ is decreased drastically over $[>AlO^-]$ with the pH. The enhanced rate values of Hg(II) adsorption is attributed to the abundance of $[>AlO^-]$ and [>AlOH] as $pH \rightarrow pH_{zpc}$.

### 3.3. Transition state of Hg(II) adsorption

The Arrhenius equation was formulated empirically, relating reaction rate and temperature. However, the Erying equation is a mechanistic construct, based on transition state theory [26]. Both equations were applied to calculate $E_a$, $\Delta H^{\#}$, $\Delta S^{\#}$ and $\Delta G^{\#}$ of Hg(II) adsorption.

As shown in Fig. 3(A and B) and in Supplementary Materials (Fig. 3S), Arrhenius plots, i.e. $-\ln(k^{ion}_{Hg(II)})$ versus $1/T$, were constructed to calculate activation energy, $E_a$ of Hg(II) adsorption on gibbsite:

$$\ln(k^{i}_{Hg(II)}) = -\frac{E_a}{RT} + \ln A \quad (2)$$

where $R$ is the universal gas constant and $A$ is an empirical constant. As shown in Table 2, the $E^1_a$ (S-1: activation energy) is greater than that of S-2 step at pH 3.1. At every other pH $E^1_a < E^2_a$. The $E^1_a$ values are in agreement with the data of metal ions adsorption on hydrous oxides [23]. However, the $E^2_a$ values (S-2: activation energy) vary between 73 and 18 kJ/mol, which signal the operation of a slow reaction step (S-2). In a given electrolyte, $E^1_a$ values showed a significant reduction with the pH (Table 2) which shows the importance of surface speciation on Hg(II) adsorption.

The enthalpy and entropy of activation ($\Delta H^{\#}$, $\Delta S^{\#}$) of Hg(II) adsorption on gibbsite were also calculated from the same data using Erying model:

$$\ln\left(\frac{k^{i}_{Hg(II)}}{T}\right) = \frac{-\Delta H^{\#}}{R}\frac{1}{T} + \frac{\Delta S^{\#}}{R} + \ln\left(\frac{k_B}{h}\right) \quad (3)$$

Table 2
Activation energy values of two-step Hg(II) adsorption on gibbsite as a function of pH and electrolyte type

| | pH | | | | | | | | | | | |
|---|---|---|---|---|---|---|---|---|---|---|---|---|
| | $NaNO_3$ | | | | $NaClO_4$ | | | | NaCl | | | |
| | 3.1 | 4.2 | 5.5 | 7.1 | 3.1 | 4.2 | 5.5 | 7.1 | 3.1 | 4.2 | 5.5 | 7.1 |
| $E_1$ [a] (kJ $mol^{-1}$) | 49 | 26 | 17 | 17 | 52 | 25 | 18 | 14 | 38 | 26 | 23 | 22 |
| $E_2$ [a] (kJ $mol^{-1}$) | 22 | 48 | 39 | 48 | 73 | 46 | 59 | 18 | 28 | 48 | 25 | 8 |

Calculations were done applying Arrhenius equation.
[a] $E_{i=1,2}$: activation energy $i$: reaction steps.

where $h$, $k_B$ and $R$ are Planck, Boltzmann, and universal gas constants, respectively. As shown in Fig. 3(A–D), the $\ln(k^i_{Hg(II)}/T)$ versus $1/T$ showed a linear relationship complying Erying model. The $\Delta H^{\#}$ and $\Delta S^{\#}$ values of activation state were calculated from the slopes and intercepts of the plots shown in Fig. 3(C and D) and the results are given in Table 3. The free energy of activation ($\Delta G^{\#}$) was derived from $\Delta G^{\#} = \Delta H^{\#} - T_{av}\Delta S^{\#}$ where $T_{av}$ is the arithmetic mean of the temperature. As shown in Table 3, always $\Delta S^{\#}$ values approximate to zero and $-T\Delta S^{\#}$ values are positive, which indicates that the activation states of Hg(II) adsorption is entropy driven.

The activation parameters of S-1 step, i.e. $E_a$, $\Delta G^{\#}$, $\Delta H^{\#}$, and $\Delta S^{\#}$ in $NaClO_4$ and $NaNO_3$ are not significantly different from each other which indicate similar mechanistic steps in surface bonding. However, such a conclusion cannot readily be made with respect to S-2 due to random variations of the data.

The thermodynamic data of Hg(II) adsorption on gibbsite at transition state showed similar values in $NaNO_3$ and $NaClO_4$. Hence, the configurations of Hg(II)-surface complexes are assumed similar both in $NaNO_3$ or $NaClO_4$. When $Cl^-$ is present, the Hg(II)-surface complexes seems to be different. Structural configurations of Hg(II)-surface complexes were elucidated by vibration spectroscopic measurements. However, these measurements were confined to pH ~6 at 298 K, presently.

### 3.4. Transmission vibration spectroscopy

As shown in Fig. 4(A–C), IR spectra were obtained for Hg(II) treated gibbsite in 0.01 M $NaNO_3$, 0.01 M $NaClO_4$ and 0.01 M NaCl at pH 6. Such spectral traces show little difference particularly at 4000–2500 $cm^{-1}$. By factor analysis, Wang and Johnston [26] have identified six OH stretching bands for gibbsite. Of the six structural OH stretching bands, peaks at 3433, 3370 and 3363 $cm^{-1}$ are considered as inter-layer hydrogen bonded OH and peaks at 3623, 3526 and 3519 $cm^{-1}$ are considered as intra-layer hydrogen bonded OH bands. Phambu et al. [27] have decomposed the IR spectrum of gibbsite in the range of 3000–4000 $cm^{-1}$ into seven components: 3378, 3395, 3430, 3450, 3515, 3528 and 3620 $cm^{-1}$. However, Weerasooriya et al. [28] have studied seven components at 3330, 3378, 3396, 3440, 3471, 3521 and 3621 $cm^{-1}$ for gibbsite (the same gibbsite samples were used in this work). Balan et al. [29] noted that the morphology of the IR spectrum is strongly depending on the shape and provenance of the gibbsite particles. Hence, the components of OH stretching frequencies for bare gibbsite were taken for the comparison with Hg(II) treated gibbsite spectra. The spectral traces of Hg(II)–gibbsite were resolved by deconvolution and the results are shown in Fig. 4(A and B). The spectra of Hg(II)–gibbsite samples were decomposed into six components instead of seven as obtained for bare gibbsite (Fig. 4(A–C)). As shown earlier [27] low frequency IR bands correspond to inter-layer OH and those of high frequency relates to intra-layer OH groups. The inter-layer OH groups seem active in surface bonding with Hg(II) (Table 4).

Despite of the electrolyte type used, the peak at 3396 $cm^{-1}$ was disappeared in all cases showing strong evidence for direct Hg(II) bonding on gibbsite surface hydroxyls. The peak com-

Table 3
Thermodynamic parameters for dynamic adsorption of Hg(II) at gibbsite–water interface as a function of pH and electrolyte type

| | $NaNO_3$ | | | $NaClO_4$ | | | NaCl | | |
|---|---|---|---|---|---|---|---|---|---|
| | $\Delta G^{\#}$ (kJ $mol^{-1}$) | $\Delta H^{\#}$ (kJ $mol^{-1}$) | $\Delta S^{\#}$ (kJ $mol^{-1}$ $K^{-1}$) | $\Delta G^{\#}$ (kJ $mol^{-1}$) | $\Delta H^{\#}$ (kJ $mol^{-1}$) | $\Delta S^{\#}$ (kJ $mol^{-1}$ $K^{-1}$) | $\Delta G^{\#}$ (kJ $mol^{-1}$) | $\Delta H^{\#}$ (kJ $mol^{-1}$) | $\Delta S^{\#}$ (kJ $mol^{-1}$ $K^{-1}$) |
| pH 3.1 | | | | | | | | | |
| S-1 | 86 | 46 | −0.122 | 86 | 50 | −0.121 | 89 | 35 | −0.180 |
| S-2 | 93 | 19 | −0.061 | 90 | 71 | −0.064 | 93 | 25 | −0.231 |
| pH 4.2 | | | | | | | | | |
| S-1 | 80 | 24 | −0.204 | 98 | 24 | −0.249 | 84 | 24 | −0.204 |
| S-2 | 87 | 45 | −0.145 | 87 | 43 | −0.147 | 89 | 45 | −0.147 |
| pH 5.5 | | | | | | | | | |
| S-1 | 80 | 15 | −0.218 | 79 | 15 | −0.213 | 86 | 20 | −0.222 |
| S-2 | 89 | 36 | −0.089 | 83 | 56 | −0.089 | 89 | 22 | −0.226 |
| pH 7.1 | | | | | | | | | |
| S-1 | 82 | 14 | −0.258 | 66 | 12 | −0.183 | 83 | 19 | −0.217 |
| S-2 | 87 | 46 | −0.247 | 88 | 15 | −0.247 | 91 | 6 | −0.288 |

Parameter calculations were made according to Erying model. S-1: fast step; S-2: slow step.

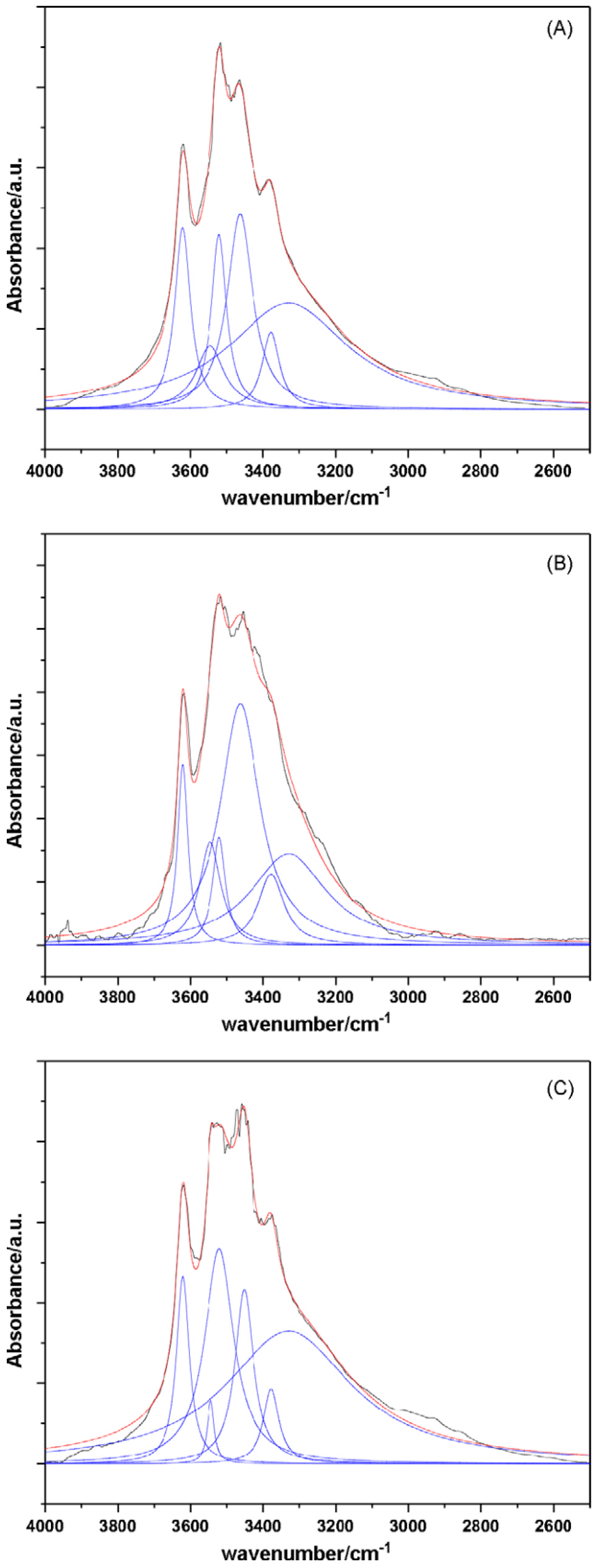


Fig. 4. Deconvoluted FT-IR spectra of Hg(II)-surface complexes. The system pH is 6. Gibbsite, 2 g $L^{-1}$; initial [Hg(II)], 2 μM; Hg(II) at 298 K. (A) $NaNO_3$; (B) $NaClO_4$; (C) NaCl.

Table 4
Deconvoluted peak components of Hg(II) treated gibbsite samples used to fit vibration spectroscopic traces obtained under transmission mode

| Gibbsite ($cm^{-1}$) | Hg(II) treated gibbsite ($cm^{-1}$) | | |
|---|---|---|---|
| | $NaNO_3$ | $NaClO_4$ | NaCl |
| 3378 | 3378 | 3378 | 3378 |
| 3380-Broad | (−50) 3330 | (−50) 3330 | (−50) 3330 |
| **3396** | **Disappeared** | **Disappeared** | **Disappeared** |
| 3440 | (+23) 3463 | (+23) 3463 | (+12) 3452 |
| 3471 | (+75) 3546 | (+75) 3546 | (+73) 3544 |
| 3521 | 3521 | 3521 | 3521 |
| 3621 | 3621 | 3621 | 3621 |

The peak components of untreated samples were taken from Ref. [28]. Irrespective of the type of electrolyte used, always the untreated gibbsite spectral traces were always resolved into seven peak components. All samples were prepared using 2 g $L^{-1}$ gibbsite and initial [Hg(II)] = 2 μM at 298 K in pH 6.

ponent at 3380 $cm^{-1}$ showed a broad band, which was shifted to 3330 $cm^{-1}$. However, the peak components at 3378, 3521 and 3621 $cm^{-1}$ remained almost same with some changes in full width at half height and the peak area. The peak components at 3440 and 3471 $cm^{-1}$ in bare gibbsite shifted to 3463 and 3546 $cm^{-1}$ for Hg(II)–gibbsite samples both in $NaNO_3$ and $NaClO_4$ which implies a similar mechanism of surface bonding. However, the relative shifting of these peaks in NaCl is somewhat different, i.e. the peaks at 3440 and 3471 $cm^{-1}$ shifted to 3452 and 3544 $cm^{-1}$, respectively. This indicates that in the presence of $Cl^-$, Hg(II) should bond to the surface differently.

## 4. Conclusions

The Hg(II) adsorption kinetics data were quantified well with pseudo-first order model at excessive concentration of surface sites. The Hg(II)–gibbsite interactions showed analogous pathways both in $NaClO_4$ and $NaNO_3$. Abundance of $HgCl_2{}^0$ species in solution was accounted for reduced Hg(II) adsorption density in the presence of chloride.

## Acknowledgements

RW thanks DAAD for Erlangen (Germany) abidance as a Guest Professor (2002–2004). International Foundation for Science (Sweden) donated the Auto-titrator to Kandy labs under AF 2407/F grant. The reviewers' comments significantly enhanced manuscript quality.

## Appendix A. Supplementary data

Supplementary data associated with this article can be found, in the online version, at doi:10.1016/j.jhazmat.2007.01.134.

## References

[1] D.R.S. O'Driscoll, N.J. Rencz, A.N. Lean, The biochemistry and fate of mercury in natural environments, in: A. Sigel, H. Sigel, R.K.O. Sigel (Eds.), Metal Ions in Biological Systems, vol. 43, Marcel Dekker, New York, 2005, pp. 281–304.

[2] K.M. Batten, K.M. Scow, Sediment microbial community composition and methyl mercury pollution at four mercury mined impacted sites, Microbial Ecol. 46 (2003) 429–441.
[3] L. Gavis, J. Ferguson, The cycling of mercury through the environment, Water Res. 6 (1972) 989–1008.
[4] UNEP, 2003 Global Assessment of Mercury: UN Environmental Program at http://www.chem.unep.ch/mercury/Report/GMA-report.TCO.htm. Viewed on 20 June 2006.
[5] W.F. Fitzgerald, D.R. Engstrom, R.P. Mason, E.A. Nater, The case for atmospheric mercury contamination in remote areas, Environ. Sci. Technol. 32 (1998) 1–7.
[6] W. Stumm, J.J. Morgan, Aquatic Chemistry: Chemical Equilibria and Rates in Natural Waters, 3rd ed., Wiley, New York, NY, 1996.
[7] E.D. Stein, Y. Cohen, A.M. Winter, Environmental distribution and transformation of mercury compounds, Crit. Rev. Environ. Sci. Technol. 26 (1996) 1–43.
[8] C. Gagon, E. Pelletier, A. Mucci, W.F. Fitzgerlald, Behavior of methylated mercury in organic rich coastal sediments, Limnol. Oceanogr. 41 (1996) 428–431.
[9] US Environmental Protection Agency, Guidance for Implementing the Methylmercury Water Quality, 2001. Available from http://www.epa.gov/waterscience/criteria/methylmercury/guidance-draft.html. Drinking water standards, 1995 (viewed on 28 October 2006).
[10] W. Stumm, Chemistry of the Solid–Water Interface, 2nd ed., Wiley–Interscience, New York, 1990.
[11] A.K. Khwaja, P.B. Bloom, P.L. Brezonik, Binding constants of divalent mercury in soil humic acids and soil organic matter, Environ. Sci. Technol. 40 (2006) 844–849.
[12] M. Hoch, R. Weerasooriya, Modeling interactions at the TBT–kaolinite interface, Chemosphere 59 (2005) 743–752.
[13] D.A. Dzombak, F.M.M. Morel, Surface Complexation Modeling: Hydrous Ferric Oxide, Wiley–Interscience, New York, 1990.
[14] D. Sarkar, M.E. Essington, K.C. Misra, Adsorption of mercury(II) by variable charge surfaces of quartz and gibbsite, Soil Sci. Am. J. 63 (1999) 1626–1638.
[15] C.S. Kim, J.J. Rytuba, G.E. Brown Jr., EXAFS study of mercury(II) sorption to Fe- and Al-(hydr)oxides. I. Effects of pH, J. Colloid Interf. Sci. 271 (2004) 1–15.
[16] C.S. Kim, J.J. Rytuba, G.E. Brown Jr., EXAFS study of mercury(II) sorption to Fe- and Al-(hydr)oxides. I. Effects of chloride and sulfate, J. Colloid Interf. Sci. 270 (2004) 9–20.
[17] R. Weerasooriya, W. Senewiratne, H.A. Kathriarachchi, H.J. Tobschall, Thermodynamic assessment of Hg(II)–gibbsite interactions, J. Colloid Interf. Sci. 301 (2006) 452.
[18] R. Weerasooriya, B. Dharamasena, AluthpatabendiF D., Copper–gibbsite interactions: an application of $1-\mathrm{p}K$ surface complexation model, Colloids Surf. 170 (2000) 65–77.
[19] R. Weerasooriya, D. Aluthpatabendi, H.J. Tobschall, Charge distribution multi-site complexation (CD-MUSIC) modeling of Pb(II) adsorption on gibbsite, Colloids Surf. 189 (2000) 131–144.
[20] M. Keizer, W.H. van Riemsdijk, ECOSAT Version 4.7, Equilibrium Calculations of Reactions and Transport, Department of Soil Science, Wagenigen Agricultural University, The Netherlands, 1999.
[21] H. Zhang, H.M. Selim, Kinetics of arsenate adsorption–desorption in soils, Environ. Sci. Technol. 39 (2005) 6101–6108.
[22] L. Axe, P.J. Trivedi, Intraparticle surface diffusion of metal contaminants and their attenuation in microporous amorphous Al, Fe, and Mn oxides, Colloid Interf. Sci. 247 (2002) 259–265.
[23] A. Wilezak, T.M. Keinath, Kinetics of sorption and desorption of copper(II) and lead(II) on activated carbon, Water Environ. Res. 65 (1993) 238–244.
[24] N. Chiron, R. Guilet, E. Deydier, Adsorption of Cu(II) and Pb(II) onto grafted silica: isotherms and kinetic models, Water Res. 37 (2003) 3079–3086.
[25] P.C. Hiemenz, Polymer Chemistry: The Basic Concepts, 1st ed., CRC Press, New York, 1984.
[26] S. Wang, C.T. Johnston, Assignment of the structural OH stretching bands on gibbsite, Am. Mineral. 85 (2000) 739–745.
[27] N. Phambu, B. Humbert, A. Burneau, Relationship between the infrared spectra and the lateral specific surface areas of gibbsite samples, Langmuir 16 (2000) 6200–6207.
[28] R. Weerasooriya, H.J. Tobschall, D. Wijesekara, E.K.A.U.K. Archachige, K.A.S. Pathiratne, On the mechanistic modeling of As(III) adsorption on gibbsite, Chemosphere 51 (2003) 1001–1013.
[29] E. Balan, M. Lazzeri, G. Morin, F. Mauri, First principles calculations of the OH stretching modes of gibbsite, Am. Mineral. 91 (2006) 115–120.